Phonons in ternary group-III nitride alloys

H. Grille and Ch. Schnittler
Institut für Physik, Technische Universität Ilmenau, PSF 100565, D-98684 Ilmenau, Germany

F. Bechstedt
Institut für Festkörpertheorie und Theoretische Optik, Friedrich-Schiller-Universität, Max-Wien-Platz 1, D-07743 Jena, Germany

(Received 28 July 1999)

The lattice dynamics of random $A_xB_{1-x}N$ alloys (A,B=Al, Ga, In) is studied with a method based on the modified random-element isodisplacement (MREI) and a rigid-ion model. The MREI description is generalized so that no additional force constants are needed but all lattice vibrations can be considered. Phonon frequencies and spectral weights are studied versus composition x for zinc-blende and wurtzite mixed crystals. The one- and two-mode behavior of the zone-center optical phonons is discussed in the light of the interplay of elastic and electric forces as well as of the atomic masses. The results are compared with data from recent Raman and IR measurements.

I. INTRODUCTION

The III-V nitride semiconductors have recently become important materials for the fabrication of optoelectronic devices operating in the green, blue, and ultraviolet spectral region.[1] This holds in particular for their ternary or pseudobinary $A_xB_{1-x}N$ alloys, e.g., $Al_xGa_{1-x}N$, $In_xGa_{1-x}N$, and $Al_xIn_{1-x}N$. Alloying among the group-III nitrides allows us, in principle, to change the band gap from about 1.9 eV in InN to 6.3 eV in AlN with an intermediate value 3.5 eV for GaN. Despite of the fact that the growth of III-N alloys has proven to be extremely challenging in the last years, there remain important questions concerning their atomic structure, the miscibility of these compounds with a common anion from the first row of the periodic table, and the characterization or spectral indication of effects like miscibility or phase separation.

Under ambient conditions AlN, GaN, and InN crystallize in the hexagonal wurtzite ($2H$) structure with the space group C_{6v}^4. Recent epitaxy of thin AlN, GaN, and InN films has been demonstrated to result in the cubic zinc-blende ($3C$) structure with space group T_d^2.[2] Remarkable progress in the synthesis of such $3C$-GaN films,[3,4] but also $3C$-AlN (Ref. 5) and $3C$-InN (Refs. 6 and 7) layers are related to the plasma-assisted molecular-beam epitaxy (MBE) on GaAs(001) or $3C$-SiC(001) substrates. Meanwhile, also ternary cubic $Al_xGa_{1-x}N$ as well as $In_xGa_{1-x}N$ layers have been deposited.[5,8,9]

Independent of the cubic or hexagonal crystal structure another important concern of the epitaxial alloy layers is the phenomenon of phase separation or clustering, more strictly the miscibility or immiscibility of two nitrides. While in the past it has been believed that nitrides are fully miscible, there are strong indications for a miscibility gap.[10–13] In a closely lattice-matched $Al_xGa_{1-x}N$ system the miscibility gap temperature was shown to be rather low[14] and, hence one may expect to have more or less a true solid solution under normal conditions. In $In_xGa_{1-x}N$ alloys, however, phase separation problems have been observed experimentally in a wide composition range.[15–17] Recently, such ordering phenomena have been also reported for the $Al_xGa_{1-x}N$ system: Instead of a random alloy, for an intermediate composition region a tendency for the formation of self-organized superlattice structures has been found.[18]

A standard method to characterize the strain and the composition in epitaxial III-N alloy layers is Raman scattering. A distinct feature of the nitrides among the tetrahedrally coordinated zinc-blende and wurtzite III-V and II-VI compounds is the polar character of the chemical bonds.[19] Therefore, strong long-range electric forces play an important role for the nitrides, particularly in the lattice vibrations that are probed by Raman spectroscopy. They give rise to an angular dispersion of optical modes. Meanwhile, Raman spectra have been recorded for $Al_xGa_{1-x}N$ solid solutions crystallizing in wurtzite structure[20–25] and zinc-blende structure[8] as well. The first studies of cubic $In_xGa_{1-x}N$ samples with low-In content have been published.[9] However, zone-center modes have been also studied using infrared (IR) reflectivity[26] and Raman spectroscopy[27,28] for hexagonal $In_xGa_{1-x}N$ mixed crystals.

In alloyed systems one important phenomenon is the mode behavior of the long-wavelength optical phonons. Pseudobinary mixed crystals $A_xB_{1-x}C$ with fully pronounced random alloy character are classified into two main classes according to the behavior of their zone-center optical phonons.[29] In the one-mode class, the frequencies vary continuously and approximately linearly with the molar fraction x of the alloy. In the case of the two-mode behavior the two sets of optical modes correspond nearly to that of the two pure crystals AC or BC that compose the alloy. These extra modes may persist very close to the end compositions, $x=0$ and $x=1$. The modes occurring in the composition region where the materials are almost pure can be usually attributed to either a local or a gap mode arising from a residual concentration of the minority component. However, the Raman spectra could be more complicated due to the appearance of defect-induced modes.[30] For solid solutions $Al_xGa_{1-x}N$ the one-mode behavior of the longitudinal optical (LO) phonons has been clearly observed,[8,20–25] in agree-

ment with predictions of model calculations.[21,25,31–33] The situation in the LO case is similar for $In_xGa_{1-x}N$. [9,26–28] However, the interpretation of the experimental findings seems to be more complicated in the frequency region of the transversal optical (TO) phonons.

In this paper, a theoretical study of the zone-center optical phonons of pseudobinary crystals $A_xB_{1-x}N$ (A,B = Al, Ga, In) with fully random alloy character is presented. In Sec. II we introduce the treatment of disorder and composition, the lattice-dynamical model, and the computational methods. In Sec. III zone-center phonon frequencies and their spectral weights are derived. The theoretical results are compared with recent experimental data and discussed in the light of the strong chemical bonds and their remarkable ionic character. Finally, in Sec. IV a brief summary is given.

II. MODEL AND METHOD

A. Atomic structure

We assume that the considered mixed systems represent ideal pseudobinary alloys or ideal ternary solid solutions $A_xB_{1-x}N$ (A,B=Al, Ga, In). Usually such solutions of III-V and II-VI compounds exhibit common structurally specific features: (i) The AB-sublattice, consisting of atoms of two types, is structurally close to a virtual crystal and nearly obeys Vegard's law. Atoms in this sublattice are randomly distributed. (ii) The N sublattice is distorted, so that nearest-neighbor (NN) distances show only a slight dependence on the composition. We omit this effect and assume, that the virtual crystals possess the same crystallographic structure—zinc-blende ($3C$) or wurtzite ($2H$)—as the pure crystals AN and BN, and that the tetrahedron structure of the surroundings of an atom is nearly conserved. This assumption of nearly ''ideal'' zinc-blende and wurtzite alloys seems to be more or less fulfilled for $Al_xGa_{1-x}N$ with practically the same covalent radii of Al and Ga.[34] In the case of $In_xGa_{1-x}N$ stronger deviations may be expected, in particular for the wurtzite alloy.[35] Nevertheless, the ideal random alloy represents an important model system and should be realized not only for smaller and larger molar fractions but also within the miscibility gap, where a decomposition into alloys with other compositions occurs.[10,11,13]

The Bravais lattices of the virtual crystals are defined by the primitive basis vectors $\mathbf{a}_1=(a_0/2)(0,1,1)$, $\mathbf{a}_2=(a_0/2)(1,0,1)$, and $\mathbf{a}_3=(a_0/2)(1,1,0)$ (zinc-blende) or $\mathbf{a}_1=a(1,0,0)$, $\mathbf{a}_2=(a/2)(-1,\sqrt{3},0)$, and $\mathbf{a}_3=c(0,0,1)$ (wurtzite) with the lattice constants a_0 ($3C$) and, respectively, a and c ($2H$). The cubic and hexagonal Cartesian coordinate systems are related against each other, so that the cubic [111] direction gives the c axis in the hexagonal case. The atomic structure of the $3C$ crystals is related to the vectors

$$\boldsymbol{\tau}_1=\frac{a_0}{4}(1,1,1), \tag{1}$$

$$\boldsymbol{\tau}_2=\frac{a_0}{4}(1,-1,-1),$$

$$\boldsymbol{\tau}_3=\frac{a_0}{4}(-1,1,-1),$$

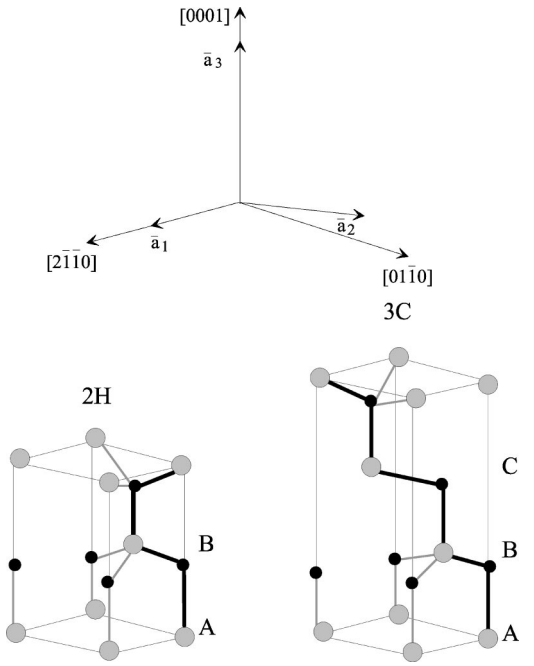

FIG. 1. Bonding and stacking sequence for the two polytypes $2H$ (wurtzite) and $3C$ (zinc-blende). Hexagonal Cartesian coordinates have been chosen.

$$\boldsymbol{\tau}_4=\frac{a_0}{4}(-1,-1,1)$$

of the ideal tetrahedron. In the unit cell there is a cation ($n=1$) at $\mathbf{r}_1=0$ and an anion ($n=2$) at $\mathbf{r}_2=\boldsymbol{\tau}_1$ (cf. Fig. 1). In the wurtzite case the tetrahedrons are slightly deformed

$$\boldsymbol{\tau}_1=(0,0,uc),$$

$$\boldsymbol{\tau}_2=\left[\frac{a}{2},\frac{a}{2\sqrt{3}},-\left(\frac{1}{2}-u\right)c\right],$$

$$\boldsymbol{\tau}_3=\left[-\frac{a}{2},\frac{a}{2\sqrt{3}},-\left(\frac{1}{2}-u\right)c\right],$$

$$\boldsymbol{\tau}_4=\left[0,-\frac{a}{\sqrt{3}},-\left(\frac{1}{2}-u\right)c\right] \tag{2}$$

and twisted by 180° around the c axis (the cubic [111] direction) according to

$$\boldsymbol{\tau}_i^*=\begin{pmatrix}-1&0&0\\0&-1&0\\0&0&1\end{pmatrix}\boldsymbol{\tau}_i. \tag{3}$$

The deviations from the ideal tetrahedrons are indicated by variations around the ideal ratio of lattice constants $c/a=\sqrt{8/3}$ and internal cell parameter $u=3/8$. In this limit the hexagonal lattice constants can be related to the corresponding cubic one by $a=a_0/\sqrt{2}$ and $c=2a_0/\sqrt{3}$. The parameter u characterizes the bond lengths parallel to the c axis (Fig. 1). Together with the two lattice contants a and c it defines the atomic coordinates in the hexagonal unit cell of the wurtzite structure. There are cations ($n=1$) in both bilayers,

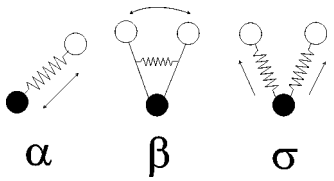

FIG. 2. Schematic representation of the three elastic short-range forces considered.

$s=1$ and $s=2$ (cf. Fig. 1) at the positions $\mathbf{r}_{11}=0$ and $\mathbf{r}_{21}=\boldsymbol{\tau}_1-\boldsymbol{\tau}_4$. The anions ($n=2$) are situated at $\mathbf{r}_{12}=\boldsymbol{\tau}_1$ and $\mathbf{r}_{22}=2\boldsymbol{\tau}_1-\boldsymbol{\tau}_4$. In the case of strain-free alloys the atomic positions $\mathbf{R}_n=\mathbf{R}+\mathbf{r}_n$ ($3C$) and $\mathbf{R}_{sn}=\mathbf{R}+\mathbf{r}_{sn}$ ($2H$) are described using Vegard's rule. Consequently, we interpolate the characteristic geometry parameters $p=a_0$, a, c, and u between the values p_{AN} and p_{BN} of the pure compounds with the molar fraction x:

$$p(x)=xp_{AN}+(1-x)p_{BN}. \tag{4}$$

Consequently, for a given composition x the atomic positions are assumed to be fixed. The nitrogen atoms are situated on the anion sublattice ($n=2$), whereas the substituted atoms A and B share the sites of the other sublattice ($n=1$). The occupation of these sites is completely random, but conserves the composition x in the average.[30]

B. Lattice-dynamical model

In order to describe the lattice dynamics of the group-III nitrides under consideration, we apply a rigid ion model. The short-range elastic forces are characterized by a three-parameter Keating model[36–38] for tetrahedrally coordinated materials. The interactions with the first-nearest-neighbor and second-nearest-neighbor atoms are characterized by a central (α,bond-stretching), a noncentral angular (β,bond-bending), and a stretch-stretch (σ) Keating force constant (cf. Fig. 2). The constant β (σ) represents an effective three-body interaction related to a change of the bond angle (length). Since we are mainly interested in the Raman frequencies, we only consider zone-center phonons with vanishing wave vector. However, the model can be also applied to the description of lattice vibrations with arbitrary wave vectors.[30] Without the self-interaction of the atoms the Fourier transformation of the force-constant matrix gives ($n,n'=1,2$; $s,s'=1,2$),

$$F^{3C}_{\alpha\alpha'}(nn'|0)=-\frac{\delta_{\alpha\alpha'}}{\sqrt{M_nM_{n'}}}\{\delta_{nn'}(\beta+2\sigma)+(1-\delta_{nn'})4(\alpha+\beta-\sigma)\}, \tag{5}$$

$$F^{2H}_{\alpha\alpha'}(sns'n'|0)=-\frac{\delta_{\alpha\alpha'}}{\sqrt{M_nM_{n'}}}\left\{\delta_{nn'}(\beta+2\sigma)\left[\delta_{ss'}\frac{9}{8}\left(\frac{\tau_{4y}^2}{|\boldsymbol{\tau}_4|^2}-\frac{\tau_{4y}^2+4\tau_{4z}^2}{|\boldsymbol{\tau}_4|^2}\delta_{\alpha z}\right)+(1-\delta_{ss'})\frac{9}{2}\frac{|\tau_{4z}|}{|\boldsymbol{\tau}_4|}\delta_{\alpha z}\right]+(1-\delta_{nn'})\left[\delta_{ss'}[3(\alpha-\beta-\sigma)\delta_{\alpha z}+2\beta]+(1-\delta_{ss'})\left(\frac{9}{2}(\alpha-\beta-\sigma)\left(\frac{\tau_{4y}^2}{|\boldsymbol{\tau}_4|^2}-\frac{\tau_{4y}^2-2\tau_{4z}^2}{|\boldsymbol{\tau}_4|^2}\delta_{\alpha z}\right)+6\beta\right)\right]\right\}. \tag{6}$$

The self-interaction terms are calculated by the sum rule due to the infinitesimal translation invariance. It follows

$$F^{3C}_{\alpha\alpha'}(nn)=\frac{\delta_{\alpha\alpha'}}{M_n}(4\alpha+5\beta-2\sigma), \tag{7}$$

$$F^{2H}_{\alpha\alpha'}(snsn)=F^{3C}_{\alpha\alpha'}(nn)+\frac{\delta_{\alpha\alpha'}}{M_n}\left\{[(4\alpha-3\beta-2\sigma)-12(\alpha-\beta-\sigma)\delta_{\alpha z}]\frac{\frac{1}{8}\tau_{4y}^2-\tau_{4z}^2}{|\boldsymbol{\tau}_4|^2}-\frac{9}{8}(\beta+2\sigma)\times\frac{|\boldsymbol{\tau}_4|^2-4|\boldsymbol{\tau}_4||\tau_{4z}|+3\tau_{4z}^2}{|\boldsymbol{\tau}_4|^2}\delta_{\alpha z}\right\}, \tag{8}$$

where $\tau_{4y}=-a/\sqrt{3}$, $\tau_{4z}=-(\frac{1}{2}-u)c$, and $|\boldsymbol{\tau}_4|^2=\tau_{4y}^2+\tau_{4z}^2$.

In expressions (6) and (8) we have resigned to generalize the force constants to the wurtzite structure. Only the deformation of the tetrahedra with $\tau_{4y}\neq\sqrt{8}\tau_{4z}$ is taken into account. In fact, in the limit of ideal tetrahedra with $u=3/8$ and $c/a=\sqrt{8/3}$, i.e., $\tau_{4y}=\sqrt{8}\tau_{4z}$, the self-interaction terms become equal for the two crystal structures. Moreover, expression (6) describes the same first- and second-NN interactions as Eq. (5), only rewritten in hexagonal coordinates. Therefore we use the same constants α, β, and σ as in the zinc-blende case. In the real wurtzite case the interaction of neighbored atoms depends on the bilayer index $s=1,2$ and, hence, differs for the interaction with upper or lower atoms. As a consequence the three Cartesian directions are not equivalent anymore. We do not apply the mass approximation[39] to the mixed crystals. Rather, we interpolate the force constants and use arithmetic mean values of the parameters of the pure crystals weighted with the composition. The structrural parameters used are given in Table I. The first sets are taken into account.

In the polar group-III nitrides the atomic displacements are accompanied by electrostatic forces. They are calculated by means of an Ewald summation.[31] The resulting Coulomb

TABLE I. Parameters of the group-III nitrides. The structural parameters c/a and u, describing the deformation of the tetrahedron in $2H$, are taken from parameter-free calculations (Refs. 19, 40, and 43) and experiment (cf. data collection in Ref. 45). The phonon frequencies (in cm^{-1}) arise from the same *ab initio* calculations (Refs. 19, 40, 43, and 44). They are compared with those from Raman studies (Refs. 7, 8, and 55). The cation masses are given in atomic units (in amu) (Ref. 34).

Parameter	AlN	GaN	InN
c/a	1.605,[a] 1.607,[b] 1.601[c]	1.626,[e] 1.631,[b] 1.627[c]	1.632,[b] 1.613[c]
u	0.382,[a] 0.382,[b] 0.382[c]	0.377,[e] 0.381,[b] 0.377[c]	0.378[b]
$\omega_{LO}(\Gamma)$	907,[a] 890,[b] 902[d]	750,[e] 746,[b] 737[g]	596,[b] 588[h]
$\omega_{TO}(\Gamma)$	662,[a] 665,[b] 655[d]	560,[e] 567,[b] 552[g]	467,[b] 455[h]
$\omega_{LO}(L)$	750,[a] 735[b]	720,[f] 708[b]	573[b]
$\omega_{TA}(L)$	230,[a] 226[b]	139,[f] 138[b]	78[b]
M_{III}	26.98	69.72	114.82

[a]Reference 19.
[b]Reference 43.
[c]Reference 45.
[d]Reference 8.
[e]Reference 40.
[f]Reference 44.
[g]Reference 55.
[h]Reference 7.

contribution to the dynamical matrix can be written as ($n,n'=1,2$; $s,s'=1,2,S$: number of bilayers in the unit cell)

$$C_{\alpha\alpha'}(sns'n'|\hat{\mathbf{Q}}) = \frac{(-1)^{n+n'}}{\sqrt{M_n M_{n'}}}\hat{f} \times \left\{ \frac{1}{S}\sum_{\mathbf{G}\neq 0} e^{-i\mathbf{G}(\mathbf{r}_{sn}-\mathbf{r}_{s'n'})}\hat{G}_\alpha \hat{G}_{\alpha'} e^{-(|\mathbf{G}|/2\gamma)^2} + \hat{Q}_\alpha \hat{Q}_{\alpha'} - \frac{\Omega_0}{4\pi}\sum_{\mathbf{R}} (1-\delta_{\mathbf{R0}}\delta_{ss'}\delta_{nn'}) \times V^F_{\alpha\alpha'}(\mathbf{R}-\mathbf{r}_{sn}-\mathbf{r}_{s'n'}) - \frac{\Omega_0}{4\pi}\delta_{ss'}\delta_{nn'}\delta_{\alpha\alpha'}\frac{4\gamma^3}{3\sqrt{\pi}} \right\}, \quad (9)$$

with

$$V^F_{\alpha\alpha'}(\mathbf{x}) = \frac{3x_\alpha x_{\alpha'} - \delta_{\alpha\alpha'}|\mathbf{x}|^2}{|\mathbf{x}|^5}\mathrm{erfc}(\gamma|\mathbf{x}|) - \frac{2\gamma}{\sqrt{\pi}|\mathbf{x}|^2}e^{-(\gamma|\mathbf{x}|)^2}\left\{ \delta_{\alpha\alpha'} - \frac{x_\alpha x_{\alpha'}}{|\mathbf{x}|^2}[2(\gamma|\mathbf{x}|)^2+3] \right\} \quad (10)$$

and the Coulomb force constant

$$\hat{f} = \frac{4\pi e^{*2}}{\Omega_0}, \quad (11)$$

where Ω_0 denotes the unit-cell volume and γ represents an arbitrary parameter that determines the convergence of the **R** and **G** sums with **G** as vectors of the reciprocal Bravais lattice. Expression (9) is valid for both the wurtzite and zinc-blende case. The crystal structure is specified by **R**, **G**, $\mathbf{r}_{sn}$, and Ω_0. For zinc-blende only one bilayer ($s,s'=1$) has to be considered. Deriving expression (9) we have assumed that each ion carries a certain effectively screened dynamic charge $(-1)^{n+1}e^*$. Preliminarily, the tensor character of this charge in wurtzite crystals (cf. Refs. 19 and 40) has been neglected. The contribution of the long-range macroscopic electric field to the dynamical matrix proportional to $\hat{Q}_\alpha \hat{Q}_{\alpha'}$ in expression (9) gives rise to an angular dependence of the polar phonon modes.[40,41] Such a dependence of the propagation direction $\hat{\mathbf{Q}}=\mathbf{Q}/|\mathbf{Q}|$ of the phonons is a consequence of the interplay with the structural anisotropy included in the short-range elastic and Coulombic contributions to the dynamical matrix.[42] Finally, we mention that the Coulomb contribution to the self-interaction has to be calculated numerically starting from the results using expression (8). Elastic and Coulomb contributions together define the total dynamical matrix $D_{\alpha\alpha'}(sns'n'|\hat{\mathbf{Q}})$.

C. Parameter fit

At least, we have to determine four parameters α, β, σ, and $\hat{f}$ to complete the lattice dynamical model in the zinc-blende case. Unfortunately, there are no four well-known frequencies for the bulk nitrides AlN, GaN, and InN, in particular not for the zinc-blende layers. For that reason, we take results of *ab initio* phonon calculations into account. For the $3C$ polytype frequencies are available for several high-symmetry points.[19,40,43,44] Since we are interested in a reliable description of Raman frequencies, we take into account the modes LO(Γ), TO(Γ), LO(L), and TA(L). Corresponding frequencies are listed in Table I together with characteristic structural parameters of the wurtzite polytypes.[19,40,43,45] The L point in the Brillouin zone (BZ) of $3C$ is of particular interest, because it is folded onto the Γ point in the BZ of $2H$. According to the folding argument the LO(L) [TA(L)] mode can be identified as the upper B_1 (lower E_2) mode in the wurtzite structure. Although B_1 is not Raman active, we take this mode [more strictly LO(L)] into the fit procedure. The use of the upper E_2 mode instead [in the cubic case TO(L)] leads to a too-tough restriction in the parameter space. The use of the parameters α, β, σ, and $\hat{f}$, which

TABLE II. Parameters of the lattice-dynamical model. The elastic Keating parameters α,β,σ and the Coulomb force constant $\hat{f}$ are given in units of N/m. The first value (second value) arises from a fit to experimental (theoretical) phonon frequencies.

Nitride	α	β	σ	$\hat{f}$
AlN	75.479 (78.41)	1.852 (2.20)	1.666 (3.71)	208.891 (208.78)
GaN	72.89 (75.38)	1.247 (1.13)	8.139 (8.39)	163.859 (171.02)
InN	51.346 (54.95)	−1.247 (−0.73)	3.753 (5.72)	103.36 (100.85)

reproduce the TO(L) frequency, gives negative frequency squares for the TA(L) modes. In order to avoid such unphysical situations, we give up the exact reproduction of the TO(L) (upper E_2 modes) within the considered four-parameter model.

In general, the experimental Γ-point frequencies are overestimated by about 1% for AlN and GaN by the results of the density-functional perturbation theory of Karch and co-workers.[19,40,44] In the case of the *ab initio* calculation of the force constants by Grossner *et al.*,[43] this overestimation is increased for TO, but is remarkably weakened for LO. The situation in the case of InN is not very clear, since the experimental frequencies scatter over a wide range. However, the Raman frequencies 588 and 457 cm^{-1} measured recently for cubic MBE samples[7] approach the theoretical values disregarding the 1% overestimation. On the other hand, the TO frequency of 490 cm^{-1} measured in another Raman experiment[46] and the LO and TO modes at 694 and 478 cm^{-1} (Ref. 26) derived from reflectance data deviate remarkably from our data. The same holds for a frozen-phonon calculation of the TO frequency of 540 cm^{-1}.[47] The older data of Ref. 26 arise in the TO case from an extrapolation of $In_xGa_{1-x}N$ values to the $x=1$ limit. The LO-phonon frequency of InN was deduced using the Brout sum rule.[26] The range of possible frequencies of the LO and TO phonons is confirmed by recent Raman studies.[48–53]

The dynamical matrix defined in Eqs. (5), (6), and (9) gives rise to the following expressions for the frequencies used in the fit procedure:[54]

$$\omega^2_{\mathrm{LO}}(\Gamma)=\frac{1}{\mu}[4(\alpha+\beta-\sigma)+2\hat{f}/3],$$

$$\omega^2_{\mathrm{TO}}(\Gamma)=\frac{1}{\mu}[4(\alpha+\beta-\sigma)-\hat{f}/3], \tag{12}$$

$$\omega^2_{\mathrm{LO/TA}}(L)=\frac{1}{2}\left\{\frac{1}{\mu}E_{+/-}\pm\left[\left(\frac{1}{M_{\mathrm{N}}}-\frac{1}{M_{\mathrm{III}}}\right)^2E^2_{+/-}+\frac{4}{M_{\mathrm{N}}M_{\mathrm{III}}}F^2_{+/-}\right]^{1/2}\right\}, \tag{13}$$

where the reduced mass

$$1/\mu=1/M_{\mathrm{III}}+1/M_{\mathrm{N}}$$

and the force-constant combinations

$$E_+=(4\alpha+5\beta-2\sigma)+2[(\beta+2\sigma)+0.287\,68\hat{f}],$$

$$E_-=(4\alpha+5\beta-2\sigma)-[(\beta+2\sigma)+0.287\,68\hat{f}],$$

$$F_+=2(\alpha+\beta-\sigma)-2[2(\alpha-\beta-\sigma)-0.556\,80\hat{f}],$$

$$F_-=2(\alpha+\beta-\sigma)+[2(\alpha-\beta-\sigma)-0.556\,80\hat{f}] \tag{14}$$

have been introduced. The mass M_{III} of the group-III atoms is also given in Table I. The nitrogen mass is $M_{\mathrm{N}}=14.01$ amu. In the fit procedure we use two different sets of frequencies for the pure crystals. Calculated frequencies are taken from Refs. 19 (AlN), 40 and 44 (GaN), and 43 (InN). The results are listed in Table II in parentheses. The Raman frequencies are taken from Refs. 8 (AlN), 55 (GaN), and 7 (InN). Since no reasonable Raman data are available for the zone-boundary phonons, they are combined with scaled theoretical values at the L point. The frequency LO(L) [TA(L)] is scaled with the ratio of the experimental and theoretical values for LO(Γ) [TO(Γ)]. From the resulting ''experimental'' frequencies a second set of parameters α, β, σ, and $\hat{f}$ of the lattice-dynamical model arises. It is also presented in Table II. The variation between the two parameter sets is weak in agreement with the small differences of about 1% in the calculated and measured phonon frequencies. Consequently, we use in the following only the set based on the ''experimental'' frequencies. Also the variation of the model parameters with the group-III atom in the nitride is weak.

The Coulomb force constant varies with the bond length d nearly as d^{-7}. This variation mainly arises from the volume dependence d^{-3} and the variation of the dielectric constant with d. On the other hand, the variation of the unscreened Born effective charge is negligible.[19,40,44] The central force constant decreases with rising bond length according to $\alpha\sim d^{-2.7}$. This is rather close to other predicted relationships, e.g., d^{-3}.[56,57] The angular force constant β is much smaller than the bond-stretching one α. The suggested ratio $\beta/\alpha\sim 0.3(1-g)$ (Refs. 56 and 57) gives values, which approach the fit parameters in Table II, if the bond ionicity g is identified with the charge asymmetry coefficient $g=0.794$ (AlN), 0.780 (GaN), and 0.853 (InN) derived from *ab initio* calculations.[58] Comparing the absolute values in Table II with parameter sets given in the literature[10,47] indicate smaller values for α and β. However, in our case we try to describe correctly the optical-phonon frequencies and not the elastic properties. Moreover, we consider a third (stretch-stretch) elastic force constant σ. Furthermore, we found that the combination $\beta+2\sigma$ follows better than β a relationship

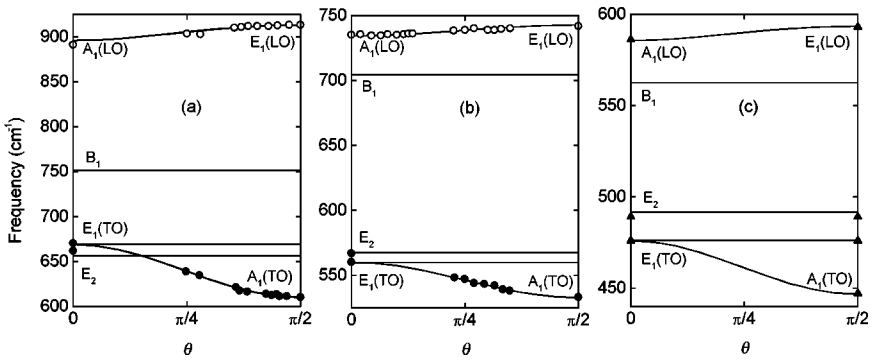

FIG. 3. Angular dispersion of the zone-center phonon frequencies of wurtzite ($2H$) nitrides, (a): AlN, (b): GaN, (c): InN. The mode symmetries E_1, A_1, B_1, and E_2 are indicated. $\hat{\mathbf{Q}}=(\sin\theta,0,\cos\theta)$ is assumed. All E_2 modes have been rigidly shifted by 15 cm^{-1} towards higher frequencies. The theoretical values are compared with experimental data (Refs. 41, 52, 53, and 59 indicated by dots and triangles.

with α of the form $(\beta+2\sigma)/\alpha\sim\frac{3}{4}(1-g)$. In any case, such relations to the bond polarity explain why the noncentral forces in the strongly ionic nitrides are so small in comparison to the central forces.

A test of the reliability of the parameters α, β, σ, and $\hat{f}$ fitted for cubic systems is the application of the lattice-dynamical model to the Γ-phonon frequencies of the wurtzite nitrides. The most sensitive test could be the angular dispersion of the LO and TO frequencies, more strictly the dependence of these frequencies on the phonon propagation direction. Since the four-parameter model neglects the crystal anisotropy, it is unable to describe correctly the angular dispersion of the frequencies. Therefore, we have replaced the parameters α and e^* by tensors with two independent diagonal elements $\alpha_\perp$ and $\alpha_\parallel$ and, respectively, $e_\perp^*$ and $e_\parallel^*$, where the directions perpendicular and parallel to the c axis are considered. We use the following small relative variations with respect to the cubic values: $(e_\perp^*-e^*)/e^*=0.015$ (0.005,0.055), $(e_\parallel^*-e^*)/e^*=0.04$ (0.03,0.01), $(\alpha_\perp^*-\alpha)/\alpha=-0.025$ ($-0.015,-0.055$), and $(\alpha_\parallel^*-\alpha)/\alpha=-0.06$ ($-0.025,-0.01$). The sequence of the values corresponds to the sequence of the nitrides AlN, GaN, and InN. The relative changes follow a chemical trend with the bond ionicity (perpendicular components) and the size of the group-III cation (parallel components). Despite their smallness of about a few percent, the variations are important to reproduce the correct angular dispersion of the modes. We note that the generalization of the radial force constant and the screened dynamical charge does not violate the C_{6v}^4 space symmetry of wurtzite crystals.

The results for the zone-center phonons of the three wurtzite nitrides are presented in Fig. 3 versus the angle θ of the phonon propagation direction with the c axis. For $\theta=0$ and $\theta=90°$ the theoretical values are compared with experimental data.[41,52,53,59] The same holds for the complete angular dispersion of the LO and one of the TO modes.[41,59] First of all, our simple lattice-dynamical model gives the correct energetical ordering of the zone-center frequencies, $E_1(\mathrm{LO})>A_1(\mathrm{LO})>B_1$. The same holds for the lower modes B_1 and E_2 that are not plotted in Fig. 3. The model also gives the correct ordering $E_1(\mathrm{TO})>E_2$ (high) for AlN. The opposite one for GaN cannot be properly reproduced. This is a consequence of the fact that the mode TO(L) of $3C$, that appears in the folded scheme of $2H$ as E_2 (high), is not used in the fit procedure. The calculated upper E_2 modes are about 15 cm^{-1} too low in frequency in comparison to the experiment. Therefore we rigidly shift the E_2-mode frequency by this value for all nitrides. This shift is already included in Fig. 3, giving a good agreement for the position of the E_2 phonons, too. The results are also extremely satisfying for the angular dispersion. The variation of the LO (lower TO) mode from its $A_1(\mathrm{LO})$ [$E_1(\mathrm{TO})$] value for $\theta=0$ to the $E_1(\mathrm{LO})$ [$A_1(\mathrm{TO})$] value for $\theta=90°$ is excellently reproduced. In the case of InN the resulting frequencies 586 cm^{-1} [$A_1(\mathrm{LO})$], 594 cm^{-1} [$E_1(\mathrm{LO})$], 476 cm^{-1} [$E_1(\mathrm{TO})$], and 447 cm^{-1} [$A_1(\mathrm{TO})$] agree exactly with the recent findings of Davydov *et al.*[52] and Harima.[53]

D. Generalized MREI model

The dependence on the composition x of ternary nitrides $A_xB_{1-x}\mathrm{N}$ ($A,B=$Al, Ga, In) and the accompanying compositional disorder are described within a generalization of the modified random-element isodisplacement (MREI) model.[30] While the original MREI model[29] has been developed to describe zone-center optical phonons in ternary-mixed zinc-blende crystals by means of additional force constants, it has been generalized to the case of arbitrary phonons and arbitrary composition profiles in zinc-blende based layered structures with tetragonal symmetry without taking into account any additional parameter.[31,32] Here we generalize the model to both zinc-blende and wurtzite alloys, to the use of an arbitrary dynamical matrix, and to an arbitrary propagation direction of the phonons. The same parameters as in the case of the pure binary compounds AN and BN are used and linearly interpolated for a given composition x.

We consider occupation numbers $\eta_j(sn\mathbf{R})=1$, if an atom of kind $j=A,B$, N and mass $M_j(n)$ is placed on an atomic site $\mathbf{R}_{sn}$, or $\eta_j(sn\mathbf{R})=0$, otherwise, and a configuration average $\langle\ldots\rangle$ with $\langle\eta_j(sn\mathbf{R})\rangle=c_j(sn)$, where $c_j(sn)$ are the concentrations of atoms of the jth species in the cation ($n=1$) or anion ($n=2$) part of the sth bilayer. In the case of the ideal alloys under consideration, it holds $c_A(sn)=\delta_{n1}x$, $c_B(sn)=\delta_{n1}(1-x)$, and $c_\mathrm{N}(sn)=\delta_{n2}$ and, respectively, $M_A(1)=M_A$, $M_B(1)=M_B$, and $M_\mathrm{N}(2)=M_\mathrm{N}$. We study the Fourier transforms $e_{j\alpha}(sn|\hat{\mathbf{Q}})$ of the configurationally averaged polarization vectors

$$e_{j\alpha}(sn|\mathbf{R}) = \langle \eta_j(sn\mathbf{R}) u_\alpha(sn\mathbf{R}) \rangle \frac{\sqrt{M_j(n)}}{\langle \eta_j(sn\mathbf{R}) \rangle} \tag{15}$$

of the atomic displacements $u_\alpha(sn\mathbf{R})$. Their motion is influenced by the Fourier transforms $h^\rho_\alpha(s|\hat{\mathbf{Q}})$ of weighted correlation functions of cation displacements and two occupation factors.[30] Following the Appendix one obtains ($j,j' = A,B,$ N; $\alpha,\alpha' = x,y,z$; $\rho = 1,2$)

$$\sum_{j',\alpha'} \left\{ \omega^2 \delta_{jj'} \delta_{\alpha\alpha'} - \frac{\delta_{jj'} - \sqrt{c_j(sn) c_{j'}(sn)}}{\sqrt{M_j(n) M_{j'}(n)}} D^{jj'}_{\alpha\alpha'}(0) \right\} e_{j'\alpha'}(sn|\hat{\mathbf{Q}})$$
$$= \sum_{j',\alpha'} \sum_{s',n'} \frac{1}{\sqrt{M_j(n) M_{j'}(n')}} D^{jj'}_{\alpha\alpha'}(sns'n'|\hat{\mathbf{Q}}) \times e_{j'\alpha'}(s'n'|\hat{\mathbf{Q}}) + \delta_{n1}(\delta_{jA} - \delta_{jB}) \sqrt{\frac{4[1-c_j(s1)]}{M_j(1) M_{\mathrm{N}}}} \times \sum_{\rho=1,2} \sqrt{1+\delta_{\rho 2}} k^\rho_s h^\rho_\alpha(s|\hat{\mathbf{Q}}), \tag{16}$$

$$\left\{ \omega^2 - \frac{1}{M_{\mathrm{N}}} D^{\mathrm{NN}}_{\alpha\alpha'}(0) \right\} h^\rho_\alpha(s|\hat{\mathbf{Q}}) = \sum_{j'} (\delta_{j'A} - \delta_{j'B}) \times \sqrt{\frac{4[1-c_{j'}(s1)]}{M_{j'}(1) M_{\mathrm{N}}}} \sqrt{1+\delta_{\rho 2}} k^\rho_s e_{j'\alpha}(sn|\hat{\mathbf{Q}}), \tag{17}$$

where $D^{jj'}_{\alpha\alpha'}(0) = D^{jj'}_{\alpha\alpha'}(snsn)$ denotes the self-interaction term that can be, in general, off-diagonal and dependent on s and n. The dependence on s, however, plays no role either for zinc-blende (because of $s=1$) or for wurtzite (because of C^4_{6v}-space-group symmetry). The force constants governing the coupling to the correlators are given as $k^1_s = \alpha + \beta - \sigma$ and $k^2_s = \alpha - \beta - \sigma - (4/\sqrt{27}\pi)\hat{f}$ and, hence, related to the well-known interatomic forces. The two indices $j,j' = A,B,$ N of the dynamical matrix of the ternary nitride indicate which sorts of atoms interact with each other. In general, averaged force constants are considered and weighted according to the composition.[32]

The model represented by the system of Eqs. (16) and (17) is generalized in several aspects. In the conventional REI approximation for polar ternary-mixed crystals with two atoms per unit cell,[29,60] more strictly speaking in the so-called modified REI approximation, the correlation functions $h^\rho_\alpha(s|\hat{\mathbf{Q}})$ have been decoupled, so that no hierarchy of equations has to be considered. The elastic forces of each end material are described by a single force constant and only the influence of the long-range electric field is taken into account. Usually additional impurity force constants are introduced to describe correctly the position of the impurity (gap or localized) modes. Here, we are using the complete dynamical matrices based on the force constants given in Table II. The additional modes are automatically included due to the consideration of the equations of motion for the correlation functions.

In the wurtzite (zinc-blende) case the system of equations of motion (16) and (17) describes [$S = 2(1)$] 30 (15) zone-center modes $\omega_\lambda(\hat{\mathbf{Q}})$ and configurationally averaged polarization vectors $e^\lambda_{j\alpha}(sn|\hat{\mathbf{Q}})$. For each composition x and propagation direction $\hat{\mathbf{Q}}$ this ensemble contains 18 (9) mixed-crystal phonon modes and a certain number of impurity modes as well as disorder-induced modes. However, the total spectral weight of all modes should be conserved and independent of the composition, i.e., equal to that of AN ($x=1$) and BN ($x=0$) crystals. The wave-vector-resolved (more strictly here, angle-resolved) one-phonon density of states can be expressed by the spectral weights $g^\lambda(\hat{\mathbf{Q}})$ according to ($\omega > 0$),

$$D(\omega|\hat{\mathbf{Q}}) = \frac{1}{6S} \sum_{\lambda=1}^{15S} 2\omega\delta[\omega^2 - \omega^2_\lambda(\hat{\mathbf{Q}})] g^\lambda(\hat{\mathbf{Q}}), \tag{18}$$

with

$$g^\lambda(\hat{\mathbf{Q}}) = \sum_{\alpha,s,n} \left\{ \sum_j c_j(sn) \left| e^\lambda_{j\alpha}(sn|\hat{\mathbf{Q}}) \right|^2 + 2\sqrt{c_A(sn) c_B(sn)} \mathrm{Re}\{ e^\lambda_{A\alpha}(sn|\hat{\mathbf{Q}}) e^{\lambda *}_{B\alpha}(sn|\hat{\mathbf{Q}}) \} \right\}. \tag{19}$$

Because of the orthonormalization of the polarization vectors it holds $\Sigma_\lambda g^\lambda(\hat{\mathbf{Q}}) = \Sigma_{\alpha,s,n} \Sigma_j c_j(sn) = 6S$. We have to mention two points. First, the same Eqs. (16)–(19) are also valid for arbitrary wave vectors not considered here. Second, the Raman intensities are not only given by the spectral weights (19). Rather, they are modified by the modulus square of a matrix element that involves the Raman tensor of the ternary alloy and, hence, depend on the light polarization vectors.

III. RESULTS AND DISCUSSION

A. One- or two-mode behavior of optical phonons

In order to study the mode behavior of the optical-phonon frequencies versus the alloy composition, we restrict our consideration to the $Al_xGa_{1-x}N$, $In_xGa_{1-x}N$, and $Al_xIn_{1-x}N$ systems and the zinc-blende polytype in a first step. In such a zinc-blende system of the type $A_xB_{1-x}C$ the pure binary crystals AC and BC only possess two Raman frequencies $\omega_{\mathrm{LO}}(AC)$, $\omega_{\mathrm{TO}}(AC)$, and $\omega_{\mathrm{LO}}(BC)$, $\omega_{\mathrm{TO}}(BC)$, respectively. There are two distinct classes of behavior of the Raman frequencies in the mixed-ternary crystals. Well known is the two-mode behavior, that is clearly realized e.g., in the case of $Al_xGa_{1-x}As$ in the frequency regions of both LO and TO phonon branches.[32] There are two LO-TO pairs, which are energetically well separated for a given composition x and degenerate to an impurity mode either at $x=1$ or $x=0$. In the one-mode case one LO-TO pair is dominant. In the clearly pronounced form of the one-mode behavior the LO- and TO-phonon frequencies shift continuously from the fre-

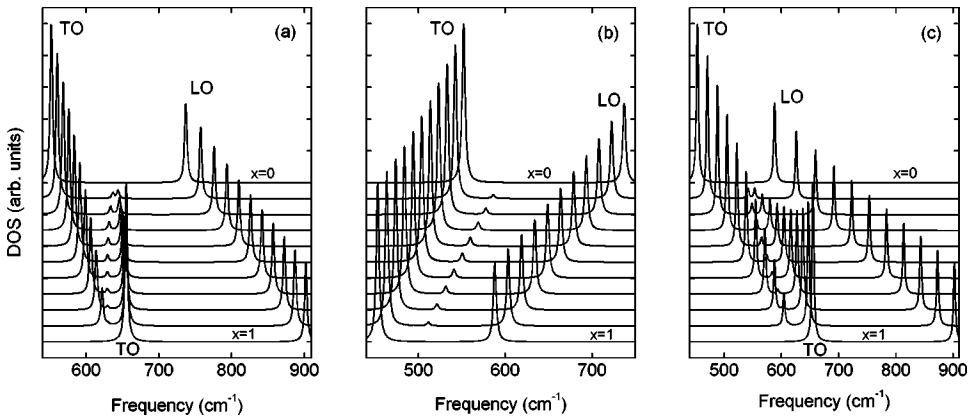

FIG. 4. Wave-vector-resolved density of states in the optical-phonon region for cubic $Al_xGa_{1-x}N$ (a), $In_xGa_{1-x}N$ (b), and $Al_xIn_{1-x}N$ (c) mixed crystals vs the composition x. The positions and weights of the zone-center phonons are calculated according to Eqs. (16), (17), and (19) using the parameters from Table II. A numerical spectral broadening of 1 cm^{-1} is assumed.

quencies of the AC crystal at $x=1$ to those of the BC crystal at $x=0$. The spectral strength of the other LO-TO pair nearly vanishes. An example for this behavior is represented by the alkali halogenide $Rb_xK_{1-x}Cl$.[61] The lattice dynamics of this alloy can be nearly described within the virtual-crystal approximation (VCA). The simplified REI models, where the elastic properties of one compound are described by only one nearest-neighbor force constant, end up in inequalitities, that have to be fulfilled for the appearance of one type of behavior.[29,60]

For instance, a clear two-mode behavior occurs for (i) a clear separation of the Γ-phonon frequencies of the two materials AC and BC. The second condition concerns (ii) a weak dispersion of the optical-phonon branches from the BZ center (Γ) to the BZ boundary (e.g., L or X). The condition of no energetical overlap also outside Γ requires certain ratios of the total pair mass and the anion mass. Whereas in $Al_xGa_{1-x}As$ the anion possesses the heaviest mass, the opposite is valid for $Al_xGa_{1-x}N$. Since the common anion possesses the smallest mass of all atoms, the AlN and GaN LO branches come close in energy and may destroy the two-mode behavior. In contrast to AlAs/GaAs system, another energetical ordering of LO and TO modes, at least for $Al_xGa_{1-x}N$ and $In_xGa_{1-x}N$, occurs and may also influence the mode behavior. This has to be studied in detail.

The actual consequences are observed in Fig. 4(a) (left panel). The two-mode behavior is destroyed for the LO phonons, whereas the TO phonons show a more complicated behavior. For $Al_xGa_{1-x}N$ only one LO phonon mode appears. Its frequency increases from that of GaN to that of AlN more or less linearly. Two TO phonon modes with remarkable spectral strength are observed. For pure binary compounds, $x=0$ and $x=1$, they change over into the impurity modes with vanishing spectral weight. Since their frequencies are below the corresponding LO phonon frequency, they represent localized modes for $x=0$ and $x=1$. In between the two TO branches one observes an additional impurity mode with a small spectral strength, that moreover vanishes close to the binary end components GaN and AlN. The behavior of the wave-vector-resolved density of states is very similar for $Al_xIn_{1-x}N$ [Fig. 4(c)] for the same reasons, since the ionic bonding and the mass differences are similar. In both cases, $Al_xGa_{1-x}N$ and $Al_xIn_{1-x}N$, the LO frequencies are larger than the TO phonon frequencies ($Al_xGa_{1-x}N$) or at least of the same order ($Al_xIn_{1-x}N$). Therefore, the two LO phonons are strongly coupled and appear as one branch in the alloy. The remarkable mass differences allows the alloy lattice to vibrate with two different TO frequencies. The situation is completely different for the $In_xGa_{1-x}N$ alloy as demonstrated in Fig. 4(b). One only observes a significant one-mode behavior. Both the LO phonon and the TO phonon vary in frequency more or less linearly between the values of GaN and InN. An additional impurity mode appears about 50 cm^{-1} above the TO frequency. However, its spectral strength is so small that it should not be observed in Raman measurements. Within a more simple MREI model one finds a one-mode behavior of TO phonon modes for both $In_xGa_{1-x}N$ and $Al_xGa_{1-x}N$.[33] In the latter case it seems to be a consequence of the simplified description neglecting any statistical correlations.

In the following figures we study the reasons for the different mode behavior in more detail in comparison with the GaAs/AlAs system. Apart from the smaller energetical separation of the GaN and AlN optical branches along the ΓL line due to their common light anion, the observations are traced back to the considerable bond ionicity, which is much larger than that of GaAs ($g=0.32$) and AlAs ($g=0.38$). Therefore, we believe that the one-mode behavior of the LO phonons is strongly affected by the accompanying electric field. In order to test this idea we show results for several smaller Coulomb force constants $\hat{f}$ of the $Al_xGa_{1-x}N$ alloy in Fig. 5. Indeed, for smaller electric forces the two-mode behavior of the LO phonons is recovered. The two-mode behavior of the TO phonons remains conserved in the entire range of considered Coulomb force constants. Below a certain critical value for $\hat{f}$ one observes groups of AlN-like and GaN-like modes. For vanishing Coulomb forces $\hat{f}=0$ the LO and TO phonons of the corresponding alloys possess the same frequency. For small $\hat{f}$ the classical two-mode behavior, well known from $Al_xGa_{1-x}As$ alloys, appears.[32] The LO-TO splitting of one material is proportional to the Coulomb force constant according to $\omega_{LO}^2(\Gamma)-\omega_{TO}^2(\Gamma)=\hat{f}/\mu$.[62] If the LO-TO splittings of the two binary end components AlN and GaN are larger than the frequency difference be-

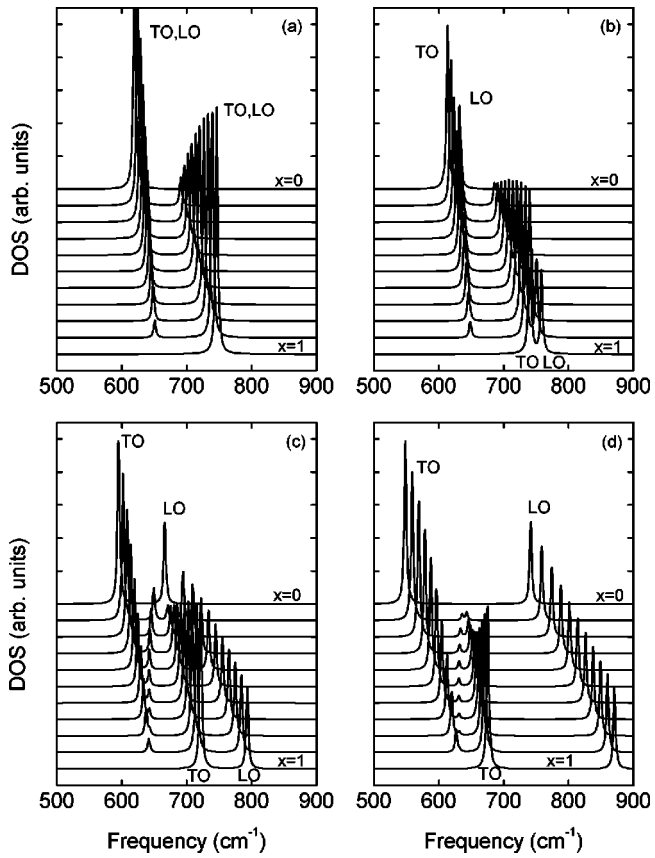

FIG. 5. Density of states of the Γ phonons in zinc-blende $Al_xGa_{1-x}N$ alloys of different compositions x. The same parameters as in Fig. 4 have been used. However, the strength of the long-range electric field has been varied between zero and the actual value of the Coulomb force constant: (a) $0\hat{f}$, (b) $0.3\hat{f}$, (c) $0.6\hat{f}$, (d) $\hat{f}$.

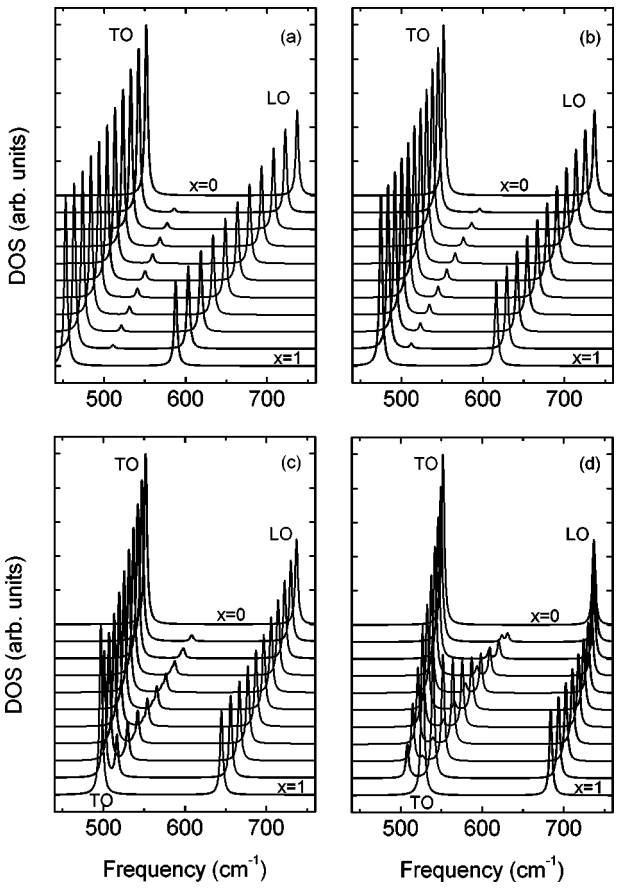

FIG. 6. Density of states of the Γ phonons in zinc-blende $In_xGa_{1-x}N$ alloys of different compositions x. The same parameters as in Fig. 4 have been used. However, the mass of the ''indium'' atom has been varied: (a) $M_{In}=114.82$ amu, (b) $M_{In}=60$ amu, (c) $M_{In}=40$ amu, (d) $M_{In}=M_{Al}=26.96$ amu.

tween the AlN-like and GaN-like TO modes, the mode behavior is destroyed. Both LO modes possess frequencies above the TO values. Because of the strong electrostatic coupling of the different AlN-like and GaN-like ''sublattices'' only one LO mode is observable. Our results are confirmed by the application[25] of the generalized dielectric model of Hon and Faust.[63] Assuming a two-mode behavior of the TO phonons the total dielectric function in the region of the optical-phonon frequencies can be expressed by a weighted sum of two oscillator dielectric functions. However, the resulting inverse dielectric function exhibits only one pole at a LO phonon frequency with a significant spectral strength. The spectral strength of the corresponding peak at lower frequencies vanishes. In contrast, the modified REI model[33] also gives only one-mode behavior for the TO-like phonons in $Al_xGa_{1-x}N$. Such an oversimplified model therefore fails in the nitride case, where two-mode behavior of the TO-like modes has been observed experimentally.[8]

Figure 6 shows the wave-vector-resolved density of states for the Γ phonons in zinc-blende $In_xGa_{1-x}N$ alloys for different masses of the ''indium'' atoms varying between the real value [Fig. 6(a)] and that for aluminum [Fig. 6(d)]. The transition from the one-mode behavior of the TO phonons in real $In_xGa_{1-x}N$ to a two-mode behavior, when the atom on an indium atomic site vibrates with the mass of an Al atom, is clearly demonstrated. The impurity mode in $In_xGa_{1-x}N$ slightly above the TO mode [cf. Figs. 6(a) and 6(b)] increases its spectral weight with decreasing cation mass on the In site. When the mass-induced splitting of the two modes is large enough, indeed two TO phonon branches occur [cf. Figs. 6(c) and 6(d)]. Our findings seem to be in qualitative agreement with the criteria for the one- or two-mode behavior derived within the framework of the modified REI model.[29] However, explicit MREI studies also give one-mode behavior for $Al_xGa_{1-x}N$.[33] Therefore, the argument that since the atomic mass of nitrogen is much smaller than Al, Ga, and In, the reduced masses of AlN, GaN, and InN are almost the same as that of N, has to be studied in more detail. The reduced mass of InN comes closer to that of GaN than to the AlN reduced mass. Consequently, a more qualitative argument seems to be more appropriate. It reads that an InN unit can easily follow the frequency of a GaN vibration, whereas this is hardly allowed for an AlN unit. This picture is also supported by the fact that if the electric force constant $\hat{f}$ (cf. discussion of Fig. 5) is reduced, a two-mode behavior of the TO modes is also recovered. The same holds for the TO modes of $Al_xGa_{1-x}N$, if $\hat{f}$ is inceased to higher values than in Fig. 5: the TO modes are shifted into similar frequency regions of that of the pure binary compounds and then show a one-mode behavior.

B. Influence of crystal structure on mode behavior

The wave-vector-resolved one-phonon densities of states resulting for the three alloys $Al_xGa_{1-x}N$, $In_xGa_{1-x}N$, and

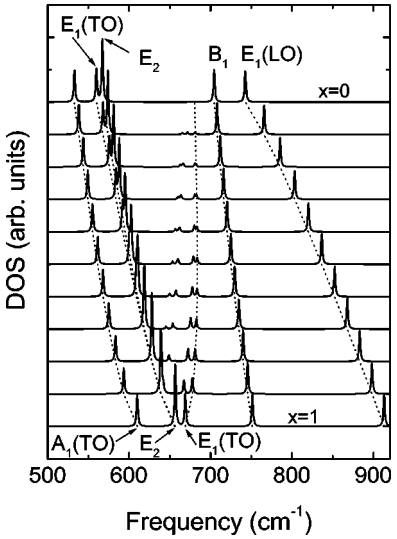

FIG. 7. Composition dependence of the spectral density of states for zone-center phonons in wurtzite $Al_xGa_{1-x}N$ mixed crystals and phonon propagation direction perpendicular to the c axis. The peak positions are indicated by dotted lines. Impurity and disorder-activated modes are not indicated by lines. A spectral broadening of 1 cm^{-1} is assumed.

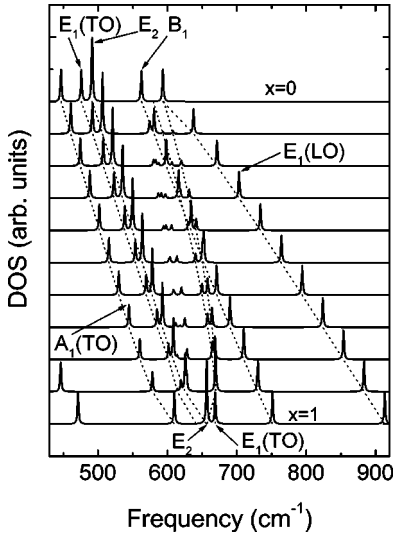

FIG. 9. Composition dependence of the spectral density of states for zone-center phonons in wurtzite $Al_xIn_{1-x}N$ mixed crystals and phonon propagation direction perpendicular to the c axis. The peak positions are indicated by dotted lines. Impurity and disorder-activated modes are not indicated by lines. A spectral broadening of 1 cm^{-1} is assumed.

$Al_xIn_{1-x}N$, which crystallize in wurtzite structure, are presented in Figs. 7, 8, and 9. According to the comparison with Raman spectra only vanishing wave vectors are considered. We restrict ourselves to the phonon propagation perpendicular to the c axis (i.e., $\theta = 90°$). Spectra for phonon propagation parallel to the c axis are not shown. In principle, the corresponding information is already included in Figs. 7, 8, and 9. For the dispersionless modes with E_2 and B_1 symmetry this is obvious. The E_1(TO) phonons are also shown. In addition the A_1(TO) phonon occurs. Instead of the A_1(LO) phonon in spectra for $\theta = 0°$ the E_1(LO) branch appears.

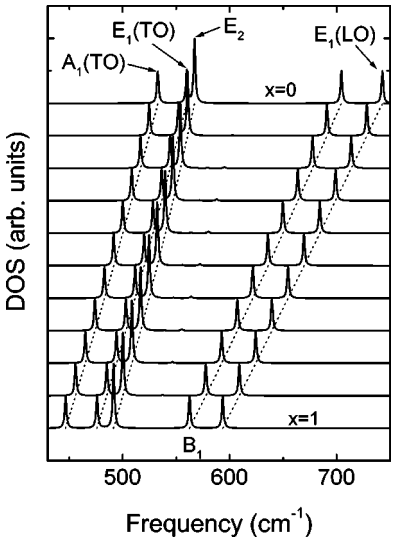

FIG. 8. Composition dependence of the spectral density of states for zone-center phonons in wurtzite $In_xGa_{1-x}N$ mixed crystals and phonon propagation direction perpendicular to the c axis. The peak positions are indicated by dotted lines. Impurity and disorder-activated modes are not indicated by lines. A spectral broadening of 1 cm^{-1} is assumed.

However, the two LO phonons appearing for $\theta = 0°$ and $\theta = 90°$ are only slightly shifted against each other in agreement with the LO angular dispersion discussed above.

The spectra of the three alloys in Figs. 7, 8, and 9 qualitatively exhibit the same behavior in the frequency range of the LO phonons. For the E_1(LO) [and also for A_1(LO), not shown] phonon and the upper-B_1 mode a significant one-mode behavior occurs. The frequencies of all modes vary almost linearly with the composition of the alloy between their values in BN and AN. The corresponding composition dependence is rather weak for the B_1 mode in $Al_xGa_{1-x}N$. This is due to its derivation from the cubic LO(L) mode, which is dominated by displacements of the common (nitrogen) anion. The stronger x dependence for $In_xGa_{1-x}N$ and $Al_xIn_{1-x}N$ is a consequence of the stronger variation of the force constants (cf. Table II). In contrast to B_1 the composition dependence of the frequency of E_1(LO) [and also A_1(LO)] shows a slight bowing with a negative bowing parameter, at least for $Al_xGa_{1-x}N$ and $Al_xIn_{1-x}N$. The entire frequency range of the LO-like phonons is free from additional impurity modes.

The one-phonon densities of states in Figs. 7, 8, and 9 are much more complicated in the frequency range related to the transverse-optical-phonon branches in the cubic crystals. This is a consequence of the weak wave-vector dispersion of the cubic TO phonon branches along the ΓL line and the two-mode behavior, at least found in the cubic case of $Al_xGa_{1-x}N$ and $Al_xIn_{1-x}N$. In the case of $In_xGa_{1-x}N$ (Fig. 8) the situation is more clear. A one-mode behavior also occurs in the TO region. The frequencies of the E_2, E_1(TO), and A_1(TO) vary more or less linearly between their values in GaN and InN. However, the frequencies are close to each other. This fact indicates the experimental difficulties to identify correctly the measured broad Raman peaks of the alloys with a phonon with a well-defined symmetry.

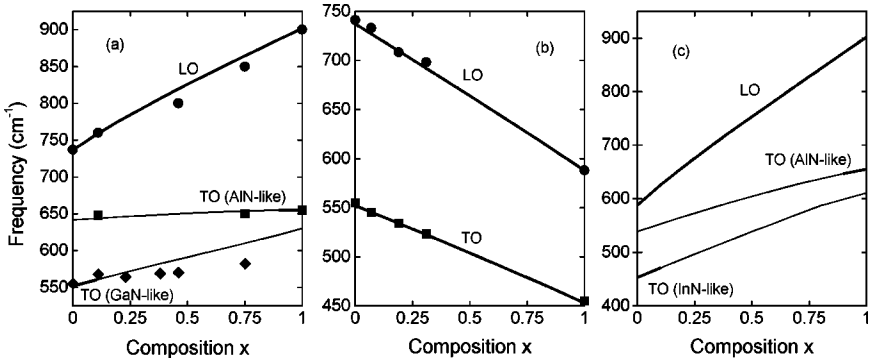

FIG. 10. Raman frequencies of $3C$-$Al_xGa_{1-x}N$ vs Al content (a) and $3C$-$In_xGa_{1-x}N$ vs In content (b). The solid lines represent the results of the calculation, thick lines indicate that the spectral strength of a mode is near 1. The dots (LO) and squares or diamonds (TO) are from Raman measurements (Refs. 8 and 55) (a) or (Ref. 9) (b). In addition, theoretical results are presented for $3C$-$Al_xIn_{1-x}N$ (c).

Disorder-activated modes do not occur in the range of the TO phonons. There is only a rather weak gap mode in between B_1 and E_2.

The situation in the case of the two other alloys is more confusing. For instance, in the case of $Al_xGa_{1-x}N$ (Fig. 7) a significant two-mode behavior is observed for TO phonons with E_1 symmetry. On the other hand, the E_2 phonons, which are derived from cubic TO(L) vibrations, as well as the TO phonon with A_1 symmetry show a one-mode behavior. The AlN-like E_1(TO) phonon has a measurable spectral weight only for compositions $x \rightarrow 1$. The composition variation of the lower GaN-like TO phonons is much stronger. Interestingly, their spectral weights keep reasonable values over a wide composition range. For $x \rightarrow 0$ the frequency of the E_1(TO) phonon is below that one of the E_2 phonon. For rising Al molar fraction the modes cross at a certain composition. E_1(TO) occurs above E_2 in the limit $x \rightarrow 1$. The one-mode behavior of the higher E_2 mode seems to be a consequence of not so different force constants of AlN and GaN and the fact that the excitation of E_2 phonons is mainly related to displacements of the two nitrogen atoms in opposite directions perpendicular to the c axis. The different behavior of the A_1(TO) and E_1(TO) phonons with respect to the mode behavior is hard to explain. Careful studies for compositions $x \rightarrow 1$ prove that the second AlN-like E_1(TO) phonon rapidly decays with the inclusion of Ga atoms in the alloy. As a consequence of this decay several impurity modes occur in between the two E_1(TO) phonon branches in the region of an expected AlN-like E_2 phonon. However, none of these little spectral structures can be really related to a second E_2 or A_1(TO) phonon. The displacement patterns belonging to these spectral features are different. The complicated behavior of the vibrating lattice of a wurtzite $Al_xGa_{1-x}N$ alloy in the spectral region of the TO phonons makes the interpretation of the experimental spectra difficult. Our prediction of the appearance of disorder-related or disorder-redistributed extra modes with different spectral weights inbetween the two E_1(TO) phonons should be related to broad spectral features in the Raman spectra.

The slightly confusing behavior of the wave-vector-resolved density of states of $2H$-$Al_xIn_{1-x}N$ in Fig. 9 arises from the crossing of the upper AlN-like E_1(TO) and E_2 branches with the B_1 phonon at intermediate compositions. The situation is additionally complicated by the weak two-mode behavior of the E_2 vibrations not occurring in the other alloys. The figure indicates the appearance of an InN-like E_2 mode for small molar fractions x whereas the more AlN-like E_2 phonon vanishes in this composition region. The strong peaks below 500 cm^{-1} correspond to lower B_1 modes.

C. Comparison with experiment

The majority of the experimental studies concern Raman measurements on the alloy system $Al_xGa_{1-x}N$.[8,20–25,55] They are supplemented by recent first-order Raman studies of $In_xGa_{1-x}N$ samples.[9,27,28] However, there are also infrared reflection investigations.[26,28,64] In principle, the available experiments confirm our theoretical predictions. This is clearly demonstrated in Fig. 10 for cubic $Al_xGa_{1-x}N$ and $In_xGa_{1-x}N$ alloy layers. The $Al_xGa_{1-x}N$ alloy layers studied experimentally were grown by a gas-source MBE on cubic $3C$-SiC substrates. The alloy layers were found to be primarily in the cubic phase and their properties exhibit a linear dependence on the Al molar fraction for $x \leqslant 0.75$. The measurements for alloy layers with $x = 0$, 0.11, 0.75, and 1 (Ref. 8) indicate an almost linear variation of the Raman frequencies with the composition x. Only one LO phonon has been observed for a given x, whereas two TO modes, one AlN-like and one GaN-like mode, occur in the corresponding frequency region. The impurity modes have not been observed at the end compositions for intensity reasons. These findings clearly confirm that the LO mode in $3C$-$Al_xGa_{1-x}N$ shows a one-mode-type behavior, whereas the TO mode consists of two branches that converge separately to respective limits. Two previous results for $x = 0.23$ and 0.38 are also presented.[55] In these backscattering measurements from a cleavage plane only GaN-like TO phonons have been observed. The reason is not clear and may be related to sample-quality problems or phase-separation tendencies.

Our theory [cf. Fig. 10(b)] is also able to describe the one-mode behavior of both the LO and TO phonons in $3C$-$In_xGa_{1-x}N$ as well as the almost linear variation of the corresponding frequencies with the composition observed in recent Raman measurements.[9] However, for the highest In content of the cubic $In_xGa_{1-x}N$ films with nominally $x = 0.31$ besides the LO Raman peak at 698 cm^{-1} also an LO peak at 625 cm^{-1} occurs. This peak indicates at least the occurrence of a second $In_xGa_{1-x}N$ phase with an In molar fraction $x = 0.8$ in agreement with the expectation of immis-

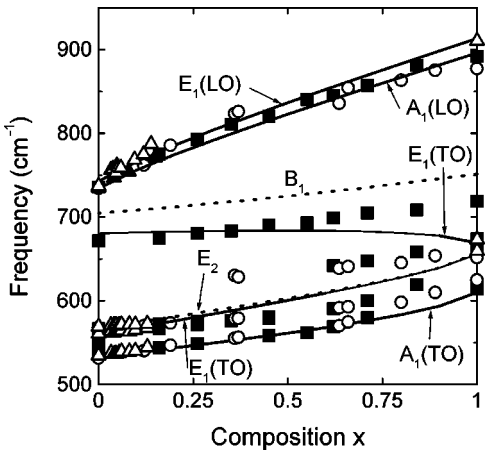

FIG. 11. Calculated (solid and dashed lines) and measured (symbols) phonon frequencies in $2H$-$Al_xGa_{1-x}N$. The theoretical mode identification is also given. The Raman data and mode frequencies from IR measurements are indicated by empty circles (Ref. 22), filled squares (Ref. 23), open triangles (Ref. 20), and filled triangles (Ref. 24).

cibility tendencies.[10–12] In addition, Fig. 10(c) shows predictions for the frequencies versus composition for the optical phonons in $3C$-$Al_xIn_{1-x}N$.

In principle, the studies of the hexagonal $Al_xGa_{1-x}N$ and $In_xGa_{1-x}N$ alloy systems[20–24,27,28] confirm the findings for the $3C$ ternary-mixed crystals. This is demonstrated in Figs. 11 and 12, where the Raman frequencies are plotted versus the alloy composition. In these figures the calculated composition dependences are compared with measured values. In addition, a similar plot is presented in Fig. 13 for $2H$-$Al_xIn_{1-x}N$. However, for this ternary nitride no experimental data exist up to now. Many more modes have to be discussed due to the larger unit cell of the wurtzite structure in comparison to the cubic case. Theoretical results are presented for all these modes and are compared with experimental peak positions in Figs. 11 and 12.

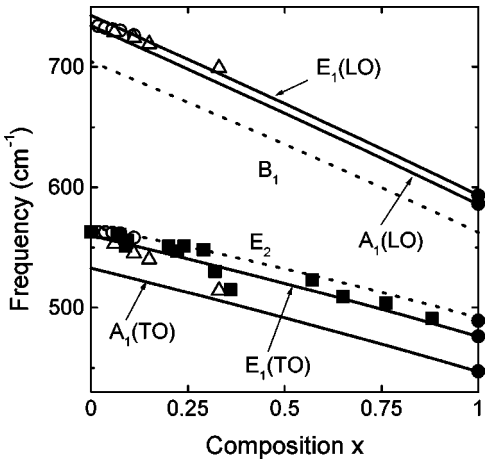

FIG. 12. Calculated and measured phonon frequencies in $2H$-$In_xGa_{1-x}N$. The theoretical mode positions (solid and dotted lines) are denoted by the mode symmetry. The experimental peak positions are indicated by filled squares (Ref. 26), open triangles (Ref. 28), open circles (Ref. 27), and filled circles (Refs. 52 and 53). The mode identification of these authors is not given.

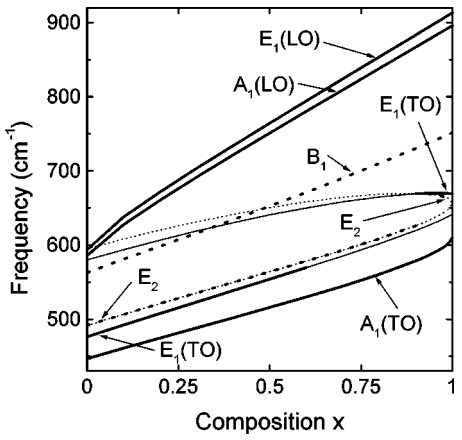

FIG. 13. Zone-center phonon frequencies vs composition x calculated for $2H$-$Al_xIn_{1-x}N$.

We begin the discussion with the $2H$-$Al_xGa_{1-x}N$ alloy (Fig. 11). There is consensus between theory and the experimental studies concerning the LO phonons.[20,22–24] The axial $A_1(\mathrm{LO})$ phonon [but also the planar $E_1(\mathrm{LO})$ mode] of mixed crystals clearly shows one-mode behavior. The absolute positions of the phonon frequencies agree widely. The almost linear composition dependence with a slight negative bowing is observed theoretically and experimentally. In the lower frequency range of the TO phonons the interpretation is more complicated concerning (i) the identification of mode symmetry, (ii) the appearance of one- or two-mode behavior, and (iii) the relation of the observed absolute values of the frequencies to other measurements or theoretical frequencies.

The mode shown as the third highest one in energy in Fig. 11 has to be identified with the B_1 symmetry. Its frequency varies nearly linearly from the GaN to the AlN value. This significant one-mode behavior has the same reason as that of the uppermost $E_1(\mathrm{LO})$ mode. According to the folding arguments the B_1 mode is related to $\mathrm{LO}(L)$ phonons in the zinc-blende case. Nominally the B_1 mode is silent and should be not observable in Raman spectra. However, in the Raman spectra of the solid solutions $Al_xGa_{1-x}N$, a weak dip was observed[23,25] close to the B_1 frequency for the whole range of composition for parallel polarizations of incident and scattered light. The authors relate their observation to alloy effects. The exact mechanism is unclear. The observed line shape is interpreted as a result of the interference between a discrete mode and a continuum of excitations. The hypothetical continuum might proceed from a breakdown of the wave-vector selection rule due to disorder in the alloy. However, there is a strong argument against the interpretation given above. The dip structure has been observed only by one group[23,25] for layers grown on top of AlN buffer layers by low-pressure metalorganic vapor-phase epitaxy (MOVPE). The dip position is about 50–70 cm^{-1} below the frequency of the upper B_1 phonon as calculated by *ab initio* methods.[19,40] Therefore, another interpretation related to the real structure of the layers is perhaps more reliable, in particular, since this dip has been observed for both GaN and AlN. The seeming agreement of the dip position with the theoretical AlN-like $E_1(\mathrm{TO})$ is not very helpful, since the spectral weight of the theoretical mode is too small.

The interpretation of Fig. 11 is also difficult in the energy regions 610–680 cm^{-1} as well as 540–580 cm^{-1}, since the Raman-allowed $E_1(TO)$ and E_2 modes come close in energy. Considering the angle dependence the lower TO mode even degenerates with the higher E_2 mode for a certain arbitrary phonon propagation direction and a certain composition x. In both frequency regions our generalization of the REI model indicates a two-mode behavior only for $E_1(TO)$ modes. The indication of two E_2 branches by Cros *et al.*[22] follows the correct identification of the E_2 phonons for alloy compositions close to that of GaN and AlN. Because of the broadening of the Raman spectra and the tendency of the alloy system for intermediate compositions to decompose into alloys with smaller and larger GaN contents the interpretation remains at least questionable. The additional problem that makes the interpretation complicated is the crossing of the E_2 graph and the lower GaN-like $E_1(TO)$ branch. We prefer another interpretation. The $A_1(TO)$ and $E_1(TO)$ phonons found for lower Al content of the samples[20,22,23,25] agree reasonably with the theoretical predictions. For $A_1(TO)$ this holds for the entire composition range both for the absolute values and the one-mode behavior. The corresponding frequency varies weakly with x until values of about $x=0.65$. Then the variation increases to reach the position of the $A_1(LO)$ frequency of AlN. The mode behavior for Al-rich $Al_xGa_{1-x}N$ alloys needs additional investigations. Theory indicates three modes: AlN-like $E_1(TO)$, E_2, and $A_1(TO)$. Experimentally[22,23] only two modes have been observed, however with frequencies in the range indicated by the theory.

In Fig. 12 the zone-center optical phonons of $2H$-$In_xGa_{1-x}N$ are plotted versus the In content of the alloys. The Raman and IR measurements have been done for MOVPE layers grown on sapphire substrates covered by buffer layers.[27,28] The agreement between theory and experiment[27,28] is excellent. In the case of the $A_1(LO)$, E_2, and $E_1(TO)$ phonons, we observe this excellent agreement not only qualitatively with respect to the composition dependence but also with respect to their absolute frequency positions in the composition range below $x=0.15$. In the case of the larger In content $x=0.33$ the discrepancies in the position of the $A_1(LO)$ and the $E_1(TO)$ phonons are increased. We trace these discrepancies back to the sample quality because of the decomposition tendency for intermediate compositions. In addition, some uncertainties up to 4 cm^{-1} due to fluctuations in the In content occur as probed by selectively excited resonant Raman scattering.[65] The theoretical results are also in reasonable agreement with the determination of the TO [probably $E_1(TO)$] phonon position in $In_xGa_{1-x}N$ synthesized by the use of electron-beam plasma technique on sapphire substrates.[26] The resulting films were polycrystalline. The frequencies have been extracted from reflectance measurements in the far-infrared spectral region.

Figure 13 summarizes the theoretical predictions for the zone-center phonons versus composition of a hypothetical $2H$-$Al_xIn_{1-x}N$ alloy. The results are rather similar to those already discussed for $Al_xGa_{1-x}N$. However, there are additional complications due to mode crossing as a consequence of the remarkable mass difference between Al and In. Moreover, E_2 also shows a two-mode behavior. The two E_2 modes converge with $x\to 1$ to nearly the same frequency position. However, for $x\to 0$ a strong InN-like E_2 mode and AlN-like one with vanishing spectral weight appear.

IV. SUMMARY

Summarizing, we have presented a generalization of the modified random-element isodisplacement model for the lattice vibrations in mixed crystals $A_xB_{1-x}N$. We also started with the idea of displacements of atoms in an effective unit cell of a mixed crystal. However, besides averaged atomic displacements, equations of motions for higher-order correlation functions have also been considered. This allows us to describe the various phonon modes in an alloyed system without taking into account additional impurity force constants. The elastic forces are derived from the constants of the final components AN and BN. The electric fields in the system are calculated via an Ewald summation. As a result, frequencies of optical phonons, impurity modes, and disorder-induced vibrations have been obtained. Their experimental relevance is described by spectral weights that are related to the eigenvectors of the generalized lattice-vibrational problem. The advantage of our generalization is the possibility of the description of arbitrary phonons in arbitrary crystal structures, whereas the modified REI model is restricted to crystals with nominally two atoms per unit cell. This progress also allowed us the discussion of the angular dispersion in alloys based on the wurtzite structure, the equilibrium crystal structure of the group-III nitrides. Moreover, in addition to the LO and TO derived phonons with E_1 and A_1 symmetry the Raman-active E_2 as well as the silent B_1 modes of wurtzite crystals have been described.

For all cubic nitride alloys we have clearly observed a one-mode behavior of the LO phonons. This behavior has been traced back to the large bond ionicities. The TO phonons exhibit either a two-mode behavior ($Al_xGa_{1-x}N$, $Al_xGa_{1-x}N$) or a one-mode behavior ($In_xGa_{1-x}N$) in dependence of the cation masses. Our results are in excellent agreement with recent Raman studies of zinc-blende nitride films. The various Raman-active modes of wurtzite alloys are also derived as functions of the composition. However, the interpretation is more complicated, in particular for $2H$-$Al_xGa_{1-x}N$. For this material the $E_1(TO)$ and E_2 phonons are close in frequency. Whereas the $A_1(TO)$ and the E_2 vibrations show a one-mode behavior, a two-mode behavior has been found for $E_1(TO)$ as for the zone-center TO phonon in the zinc-blende case. In addition, we discussed the appearance of a peak close to the silent B_1 mode in Raman spectra of $Al_xGa_{1-x}N$ wurtzite alloys by a disorder activation or another disorder-related mechanism giving rise to gap modes. Also, in the hexagonal case the agreement with the experimental findings is satisfying. In particular, the theoretical results give an opportunity for a correct identification of vibrational modes of the alloys.

ACKNOWLEDGMENTS

Various discussions with H. Harima, J.R. Leite, M.A. Renucci, and N. Wieser are acknowledged. This work was supported by the Deutsche Forschungsgemeinschaft under Grant No. Be 1346/8-4.

APPENDIX: DERIVATION OF EQUATIONS OF MOTION

We generalize the derivation of equations of motion of a mixed crystal given in Ref. 30 to the case of a more complete dynamical matrix and wurtzite symmetry. The interesting quantities are the averaged atomic displacements $v_{j\alpha}(sn\mathbf{R}) = [1/\sqrt{M_j(n)}]e_{j\alpha}(sn|\mathbf{R})$ and correlation functions $w_{jj'\alpha}(sn\mathbf{R}|s'n'\mathbf{R}')$ [Eq. (8) in Ref. 30] of fluctuations in the site occupation and the atomic-dependent displacement. The right-hand side of the equations of motion of the latter quantities is decoupled [Eq. (10) in Ref. 30] and long-range correlations in the site occupation are neglected in agreement with the assumed random alloy. Within the first-nearest neighbor approximation it holds $w_{jj'\alpha}(sn\mathbf{R}|s'n'\mathbf{R}') = \delta_{n1}\delta_{n'2}(\delta_{jA}+\delta_{jB})\delta_{j'\mathrm{N}}w_{j\mathrm{N}\alpha}(s1\mathbf{R}|s'2\mathbf{R}')$. The first-nearest nitrogen neighbors of a cation at $\mathbf{R}_{1n\mathbf{R}}$ are situated at $\mathbf{R}_{2n'\mathbf{R}'} = \mathbf{R}_{1n\mathbf{R}} + \boldsymbol{\tau}_i$ $(i=1,\ldots,4)$, where $\boldsymbol{\tau}_i$ are the vectors of the deformed tetrahedron. The force constant matrix $D^{jj'}_{\alpha\alpha'}(sn\mathbf{R}-s'n'\mathbf{R}')$ is that of an ordered system but depends on the occupation of an atomic site with a certain atomic species. It includes the elastic and electrostatic forces. From Eqs. (7)–(9) (Ref. 30) it follows

$$\sum_{\alpha'}\{\omega^2 M_j(n)\delta_{\alpha\alpha'} - D^{jj'}_{\alpha\alpha'}(0)\}v_{j\alpha'}(sn\mathbf{R}) = \sum_{\alpha',j'}\sum_{s',n',\mathbf{R}}{}' D^{jj'}_{\alpha\alpha'}(sn\mathbf{R}-s'n'\mathbf{R}') \times c_{j'}(s'n')v_{j'\alpha'}(s'n'\mathbf{R}') + (\delta_{jA}+\delta_{jB}) \times \sum_{\alpha'}\sum_{i=1}^{4} D^{j\mathrm{N}}_{\alpha\alpha'}(-\boldsymbol{\tau}_i)w_{j\mathrm{N}\alpha'}(s1\mathbf{R}|s'2\mathbf{R}'), \quad \text{(A1)}$$

$$\sum_{\alpha'}\{\omega^2 M_{\mathrm{N}}\delta_{\alpha\alpha'} - D^{\mathrm{NN}}_{\alpha\alpha'}(0)\}w_{j\mathrm{N}\alpha'}(s1\mathbf{R}|s'2\mathbf{R}') = \sum_{\alpha',j'} D^{\mathrm{N}j'}_{\alpha\alpha'}(\boldsymbol{\tau}_i)[\delta_{jj'} - c_{j'}(s1)]v_{j'\alpha'}(s1\mathbf{R}). \quad \text{(A2)}$$

These equations are translational invariant and allow us to introduce a ''pseudoelementary'' cell[66] with weighted cation of each type A and B at one cation site.

Neglecting the small anisotropy in α and e^*, the eight different nearest-neighbor correlation functions (for a given Cartesian component) can be related to two new functions $\hat{h}^{\rho}_{\alpha}(s\mathbf{R})$ with $\rho=1,2$ by

$$-(\delta_{jA}-\delta_{jB})[1-c_j(s1)]\hat{h}^1_{\alpha}(s\mathbf{R}) = \sum_{i=1}^{4} w_{j\mathrm{N}\alpha}(s1\mathbf{R}|s'2\mathbf{R}') \quad \text{(A3)}$$

and

$$-(\delta_{jA}-\delta_{jB})[1-c_j(s1)]\hat{h}^2_{\alpha}(s\mathbf{R}) = \sum_{\alpha'}\sum_{i=1}^{4} T^i_{\alpha\alpha'}w_{j\mathrm{N}\alpha'}(s1\mathbf{R}|s'2\mathbf{R}'), \quad \text{(A4)}$$

with the geometry factor of the nearest-neighbor tetrahedron $T^i_{\alpha\alpha'} = 3\tau_{i\alpha}\tau_{i\alpha'}/|\boldsymbol{\tau}_i|^2 - \delta_{\alpha\alpha'}$.

The translational invariance of the configurationally averaged ternary system with ''pseudoelementary'' cells allows Fourier transformations of the forms

$$v_{j\alpha}(sn\mathbf{R}) = \frac{1}{\sqrt{M_j(n)c_j(sn)}}\sum_{\mathbf{Q}} e^{i\mathbf{QR}}e_{j\alpha}(sn|\mathbf{Q}) \quad \text{(A5)}$$

and

$$\hat{h}^{\rho}_{\alpha}(s\mathbf{R}) = \sqrt{\frac{4(1+\delta_{\rho 2})}{M_{\mathrm{N}}c_j(s1)[1-c_j(s1)]}}\sum_{\mathbf{Q}} e^{i\mathbf{QR}}h^{\rho}_{\alpha}(s|\mathbf{Q}). \quad \text{(A6)}$$

By means of the relations (A3)–(A6) the equations of motion (A1) and (A2) can be transformed into Eqs. (16) and (17) in Sec. II D.

[1] S. Nakamura, *The Blue Laser Diode–GaN based Light Emitters and Lasers* (Springer, Berlin, 1997).

[2] M. J. Paisley, Z. Sitar, J. B. Posthill, and R. F. Davies, J. Vac. Sci. Technol. A **7**, 701 (1989).

[3] O. Brandt, H. Yang, B. Jenichen, Y. Suzuky, L. Däweritz, and K. Ploog, Phys. Rev. B **52**, R2253 (1995).

[4] D. Schikora, M. Hankeln, D. J. As, K. Lischka, T. Litz, A. Waag, T. Buhrow, and F. Henneberger, Phys. Rev. B **54**, R8381 (1996).

[5] H. Okumura, H. Hamaguchi, T. Koizumi, K. Balanishi, T. Nagatomo, and S. Yoshida, J. Cryst. Growth **189/190**, 390 (1998).

[6] A. P. Lima, A. Tabata, J. R. Leite, S. Kaiser, D. Schikora, B. Schöttker, T. Frey, D. J. As, and K. Lischka, J. Cryst. Growth **201-202**, 396 (1999).

[7] A. Tabata, A. P. Lima, L. K. Teles, L. M. R. Scolfaro, J. R. Leite, V. Lemos, B. Schöttker, T. Frey, D. Schikora, and K. Lischka, Appl. Phys. Lett. **74**, 362 (1999).

[8] H. Harima, T. Inoue, S. Nakashima, H. Okumura, Y. Ishida, S. Yoshida, T. Koizumi, H. Grille, and F. Bechstedt, Appl. Phys. Lett. **74**, 191 (1999).

[9] A. Tabata, J. R. Leite, A. P. Lima, E. Silveira, V. Lemos, T. Frey, D. J. As, D. Schikora, and K. Lischka, Appl. Phys. Lett. **75**, 1095 (1999).

[10] I. Ho and G. B. Stringfellow, Appl. Phys. Lett. **69**, 2701 (1996); J. Cryst. Growth **178**, 1 (1997).

[11] M. van Schilfgaarde, A. Sher, and A.-B. Chen, J. Cryst. Growth **178**, 8 (1997).

[12] T. Matsuoka, Appl. Phys. Lett. **71**, 105 (1997).

[13] V. A. Elyukhin and S. A. Nikishin, Semicond. Sci. Technol. **11**, 917 (1998).

[14] E. A. Albanesi, W. R. L. Lambrecht, and B. Segall, Phys. Rev. B **48**, 17 841 (1993).

[15] R. Singh, D. Doppalapudi, T. D. Moustakas, and L. T. Romano, Appl. Phys. Lett. **70**, 1089 (1997).

[16] A. Wakahara, T. Tokuda, X.-Z. Dang, S. Noda, and A. Sasaki, Appl. Phys. Lett. **71**, 906 (1997).
[17] M. D. McCluskey, L. T. Romano, B. S. Krusor, D. P. Bour, N. M. Johnson, and S. Brennan, Appl. Phys. Lett. **72**, 1730 (1998).
[18] B. Neubauer, A. Rosenauer, D. Gerthsen, O. Ambacher, M. Stutzmann, M. Albrecht, and H. P. Strunk, Mater. Sci. Eng., B **59**, 182 (1999); B. Neubauer, A. Rosenauer, D. Gerthsen, O. Ambacher, and M. Stutzmann, Appl. Phys. Lett. **73**, 930 (1998).
[19] K. Karch and F. Bechstedt, Phys. Rev. B **56**, 7404 (1997).
[20] K. Hayashi, K. Itoh, N. Sawaki, and I. Akasaki, Solid State Commun. **77**, 115 (1991).
[21] F. Demangeot, J. Frandon, M. A. Renucci, C. Meny, O. Briot, and R. L. Aulombard, J. Appl. Phys. **82**, 1305 (1997).
[22] A. Cros, H. Angerer, R. Handschuh, O. Ambacher, and M. Stutzmann, Solid State Commun. **104**, 35 (1997).
[23] S. Clur, O. Briot, J.-L. Rouviere, A. Andonet, Y.-M. Le Vaillant, B. Gil, R. L. Aulombard, J. F. Demangeot, J. Frandon, and M. Renucci, Mater. Res. Soc. Symp. Proc. **462**, 23 (1997).
[24] D. Behr, R. Niebuhr, J. Wagner, K.-H. Bachem, and U. Kaufmann, Appl. Phys. Lett. **70**, 363 (1997).
[25] F. Demangeot, J. Groenen, J. Frandon, M. A. Renucci, O. Briot, S. Clur, and R. L. Aulombard, Appl. Phys. Lett. **72**, 2674 (1998).
[26] K. Osamura, S. Naka, and Y. Murakami, J. Appl. Phys. **46**, 3432 (1975).
[27] D. Behr, R. Niebuhr, H. Obloh, J. Wagner, K. H. Bachem, and U. Kaufmann, Mater. Res. Soc. Symp. Proc. **468**, 213 (1997).
[28] N. Wieser (private communication).
[29] I. F. Chang and S. S. Mitra, Adv. Phys. **20**, 359 (1971).
[30] F. Bechstedt, H. Gerecke, and H. Grille, Phys. Rev. B **47**, 13 540 (1993).
[31] H. Grille and F. Bechstedt, Superlattices Microstruct. **16**, 29 (1994).
[32] H. Grille and F. Bechstedt, J. Raman Spectrosc. **27**, 201 (1996).
[33] S. G. Yu, K. W. Kim, L. Bergman, M. Dutta, M. A. Stroscio, and J. M. Zavada, Phys. Rev. B **58**, 15 283 (1998).
[34] *Table of Periodic Properties of Elements* (Sargent-Welch, Skokie, IL, 1980).
[35] L. Bellaiche and A. Zunger, Phys. Rev. B **57**, 4425 (1998).
[36] P. N. Keating, Phys. Rev. **145**, 637 (1966).
[37] V. J. B. Torres and A. M. Stoneham, *Handbook of Interatomic Potentials. III. Semiconductors* (Harwell Lab, Theoretical Physics Division, Harwell, 1985).
[38] G. P. Srivastava, *The Physics of Phonons* (Adam Hilger, Bristol, 1990).
[39] K. Kunc and H. Bilz, Solid State Commun. **19**, 1927 (1976).
[40] K. Karch, J.-M. Wagner, and F. Bechstedt, Phys. Rev. B **57**, 7043 (1998); (unpublished).
[41] L. Filippidis, H. Siegle, A. Hofmann, C. Thomsen, K. Karch, and F. Bechstedt, Phys. Status Solidi B **198**, 621 (1996).
[42] S.-F. Ren, H. Chu, and Y.-C. Chang, Phys. Rev. B **37**, 8899 (1988).
[43] U. Grossner, J. Furthmüller, and F. Bechstedt, Phys. Rev. B **58**, R1722 (1998).
[44] K. Karch, F. Bechstedt, and T. Pletl, Phys. Rev. B **56**, 3560 (1997).
[45] A. F. Wright and J. S. Nelson, Phys. Rev. B **51**, 7866 (1995).
[46] T. Inushima, A. Nagase, A. Iso, T. Yaguchi, and T. Shiraishi, in *Proceedings of 6th International Conference on Silicon Carbide and Related Materials* (Institute of Physics, London, 1996.)
[47] K. Kim, W. R. L. Lambrecht, and B. Segall, Phys. Rev. B **53**, 16 310 (1996).
[48] H.-J. Kwon, Y.-H. Lee, O. Miki, H. Yamano, and A. Yoshida, Appl. Phys. Lett. **69**, 937 (1996).
[49] J. S. Dyck, K. Kash, K. Kim, W. R. L. Lambrecht, C. C. Hayman, A. Argoitia, M. T. Grossner, W. L. Zhou, and J. C. Angus, Mater. Res. Soc. Symp. Proc. **482**, 549 (1998).
[50] M.-C. Lee, H.-C. Lin, Y.-C. Pan, C.-K. She, J. Ou, W.-H. Chen, and W.-K. Chen, Appl. Phys. Lett. **73**, 2606 (1998).
[51] D. R. T. Zahn (private communication).
[52] V. Yu. Davydov, V. V. Emtsev, I. N. Goncharuk, A. N. Smirnov, V. D. Petrikov, V. V. Mamutin, V. A. Vekshin, S. V. Ivanov, M. B. Smirnov, and T. Inushima, Appl. Phys. Lett. **75**, 3297 (1999).
[53] H. Harima, E. Kurimoto, Y. Sone, S. Nakashima, S. Chu, A. Ashida, and H. Fujiyasu, Phys. Status Solidi B **216**, 785 (1999).
[54] H. Grille, Ph.D. thesis, Friedrich-Schiller-Universität Jena, 1996.
[55] H. Harima, T. Inoue, S.-I. Nakashima, H. Okumura, Y. Ishida, S. Yoshida, and H. Hamaguchi, J. Cryst. Growth **189/190**, 435 (1998).
[56] T. N. Morgan and M. Maier, Phys. Rev. Lett. **27**, 1200 (1971).
[57] R. M. Martin, Phys. Rev. B **1**, 4005 (1970).
[58] A. Garcia and M. L. Cohen, Phys. Rev. B **47**, 4215 (1993).
[59] H. Siegle, G. Kaczmarczyk, L. Filippidis, A. P. Litvinchuk, A. Hoffmann, and C. Thomsen, Phys. Rev. B **55**, 7000 (1997); H. Siegle, Ph.D. thesis, TU Berlin, 1998.
[60] I. F. Chang and S. S. Mitra, Phys. Rev. **172**, 924 (1968); Phys. Rev. B **2**, 1215 (1980).
[61] X. Wang and X. X. Liang, Phys. Rev. B **42**, 8915 (1990).
[62] M. Born and K. Huang, *Dynamical Theory of Crystal Lattices* (Clarendon Press, Oxford, 1954).
[63] D. T. Hon and W. L. Faust, J. Appl. Phys. **1**, 241 (1973).
[64] P. Wiesniewski, W. Knap, J. P. Malzac, J. Camassel, M. D. Bremser, R. F. Davis, and T. Suski, Appl. Phys. Lett. **73**, 1760 (1998).
[65] N. Wieser, O. Ambacher, H. P. Felsl, L. Görgens, and M. Stutzmann, Appl. Phys. Lett. **74**, 3981 (1999).
[66] S. C. Varshney, J. F. Vetelino, S. S. Mitra, and J. F. Chang, Phys. Rev. B **12**, 5912 (1975).